Soft Matter

COMMUNICATION

View Article Online
View Journal | View Issue

Open Access Article. Published on 14 June 2022. Downloaded on 11/5/2025 4:19:57 PM.
This article is licensed under a Creative Commons Attribution 3.0 Unported Licence.

Check for updates

Cite this: *Soft Matter*, 2022, **18**, 5021

Received 4th June 2022,
Accepted 14th June 2022

DOI: 10.1039/d2sm00739h

rsc.li/soft-matter-journal

Protein corona alters the mechanisms of interaction between silica nanoparticles and lipid vesicles†

Marcos Arribas Perez [a] and Paul A. Beales *[ab]

The use of nanoparticles (NPs) for biomedical applications implies their delivery into the organism where they encounter biological fluids. In such biological fluids, proteins and other biomolecules adhere to the surface of the NPs forming a biomolecular corona that can alter significantly the behaviour of the nanomaterials. Here, we investigate the impact of a bovine serum albumin corona on interactions between silica nanoparticles (SNPs) of two different sizes and giant lipid vesicles. The formation of the protein corona leads to a significant increase of the hydrodynamic size of the SNPs. Confocal microscopy imaging shows that the protein corona alters the morphological response of vesicles to SNPs. In addition, Laurdan spectral imaging show that the protein corona weakens the effect of SNPs on the lipid packing in the GUV membrane. Our results demonstrate that a protein corona can change the interaction mechanism between nanoparticles and lipid membranes.

Silica nanoparticles (SNPs) are of biomedical interest,[1] making it important to understand the behaviour of these nanomaterials when exposed to biological media. Cell membranes rarely encounter bare nanomaterials but NPs coated by biomolecules present in biological fluids that deeply modify their physicochemical properties and biological interactions.[2,3] The major and most extensively studied component of such coatings are proteins, which form the protein corona.

Current knowledge about the impact of protein coronas on the interaction of NPs with biological membranes, and hence the potential impact on biomedical functionality and cytotoxicity that arise, still presents considerable gaps. From a toxicological perspective, it is generally accepted that protein coronas improve the biocompatibility of NPs and thereby reduce their potentially hazardous effects.[4] For instance, it has been observed that protein coronas protect cells from the cytotoxic effect induced by bare positively charged polystyrene NPs.[5] The adsorption of proteins can also minimise the toxicity by preventing the aggregation and degradation that some types of NPs experience when suspended in aqueous solutions.[6–8] On the contrary, the protein corona has been reported to increase the cellular uptake of AgNPs which, once internalised in the cells, produce severe cytotoxic effects.[9,10]

The myriad of parameters influencing the non-specific biomolecular coating of nanomaterials leads to highly complex and variable coronas formed under different experimental conditions, which makes it difficult to extract unified conclusions.[11] Protein coronas are thought to be dynamic structures where some proteins bind irreversibly to the NP surface (hard corona) but others with a weaker binding affinity (soft corona) show a dynamic and reversible attachment and detachment from the protein corona.[2,12,13] The structure and composition of the protein corona as well as the state of the proteins that form it is not yet clear and shows great variability.[12] For instance, the analysis of protein coronas formed on SNPs and polystyrene NPs have revealed more than 100 different types of proteins among which the most abundant are albumin, apolipoproteins, and hemoglobin subunits.[3,14,15] Understanding protein corona formation and their influence on NP stability, reactivity and biocompatibility is therefore an extremely challenging task requiring the combination of different experimental perspectives. In this context, reductionist studies represent a first step to provide fundamental information on structural and dynamical aspects of protein corona assembly, their influence on NP stability and their interactions with biological membranes.

Here we studied the effect of a protein corona on the interplay between SNPs of two different sizes and DOPC giant unilamellar vesicles (GUVs). To mimic the protein coverage experienced by NPs in biological media, we incubated the SNPs with Bovine Serum Albumin (BSA) proteins, a major constituent of blood plasma and cell culture media. This leads to a simplified protein corona made exclusively of BSA, which provides information about changes in non-specific interactions between

[a] *Astbury Centre for Structural Molecular Biology and School of Chemistry, University of Leeds, Leeds, LS2 9JT, UK. E-mail: p.a.beales@leeds.ac.uk*
[b] *Bragg Centre for Materials Research, University of Leeds, Leeds, LS2 9JT, UK*

† Electronic supplementary information (ESI) available: Materials and methods, NP characterisation data. Confocal microscopy images of control GUVs exposed to 0.25 mg ml^{-1} BSA. See DOI: https://doi.org/10.1039/d2sm00739h

Open Access Article. Published on 14 June 2022. Downloaded on 11/5/2025 4:19:57 PM.
This article is licensed under a Creative Commons Attribution 3.0 Unported Licence.

both types of SNPs and the lipid membranes induced by the surface coating of the NPs with proteins. We prepared initial stocks of 10 mg ml^{-1} SNPs suspended in a solution of 100 mg ml^{-1} BSA in the experimental buffer (20 mM HEPES, 150 mM NaCl, pH 7.4). The concentration of BSA (100 mg ml^{-1}) used to prepare the BSA-coated SNPs (SNPs@BSA) is comparable to the total concentration of proteins in blood serum. The stock solutions were incubated at 4 °C for 24 h (unless otherwise specified) and then diluted into experimental samples at the desired concentrations.

We first characterised the size, shape and surface charge of the SNPs before incubation with BSA. Transmission electron microscopy (TEM) images show that the two types of bare SNPs are roughly spherical but they differ in their size: the first type (Ludox SM or SNPs-18) has a diameter of nearly 18 nm (17.8 ± 4.8 nm) and the diameter of the second class (Ludox TM or SNPs-30) is around 30 nm (30.8 ± 3.9 nm) (Fig. S1a and b, ESI†). We observe a similar size distribution by DLS: 24.9 ± 0.9 nm for SNPs-18 and 43.0 ± 1.4 nm for SNPs-30(Fig. 1(a) and (b)), where the small increase in size compared to TEM is accounted for by DLS measuring the hydrodynamic diameter of the NPs. DLS also shows that both kinds of SNPs are colloidally stable in the experimental buffer for at least 48 h (Fig. S2a and b, ESI†). The ζ-potential shows that SNPs-30 are slightly more negatively charged (−18.2 ± 1.8 mV) than SNPs-18 (−15.8 ± 0.4 mV) (Fig. S2c, ESI†).

To confirm the formation of the BSA corona around the SNPs, we measured the hydrodynamic diameter of the SNPs after 1 h, 24 h and 48 h of incubation in the BSA solution. The hydrodynamic size of SNPs-18@BSA rises to 58.8 ± 2.6 nm after 1 h in the BSA solution (Fig. S2a, ESI†). SNPs-30@BSA show similar behaviour with an increment to 82.9 ± 3.1 nm (Fig. S2b, ESI†). This increase in size observed in the DLS data arises from

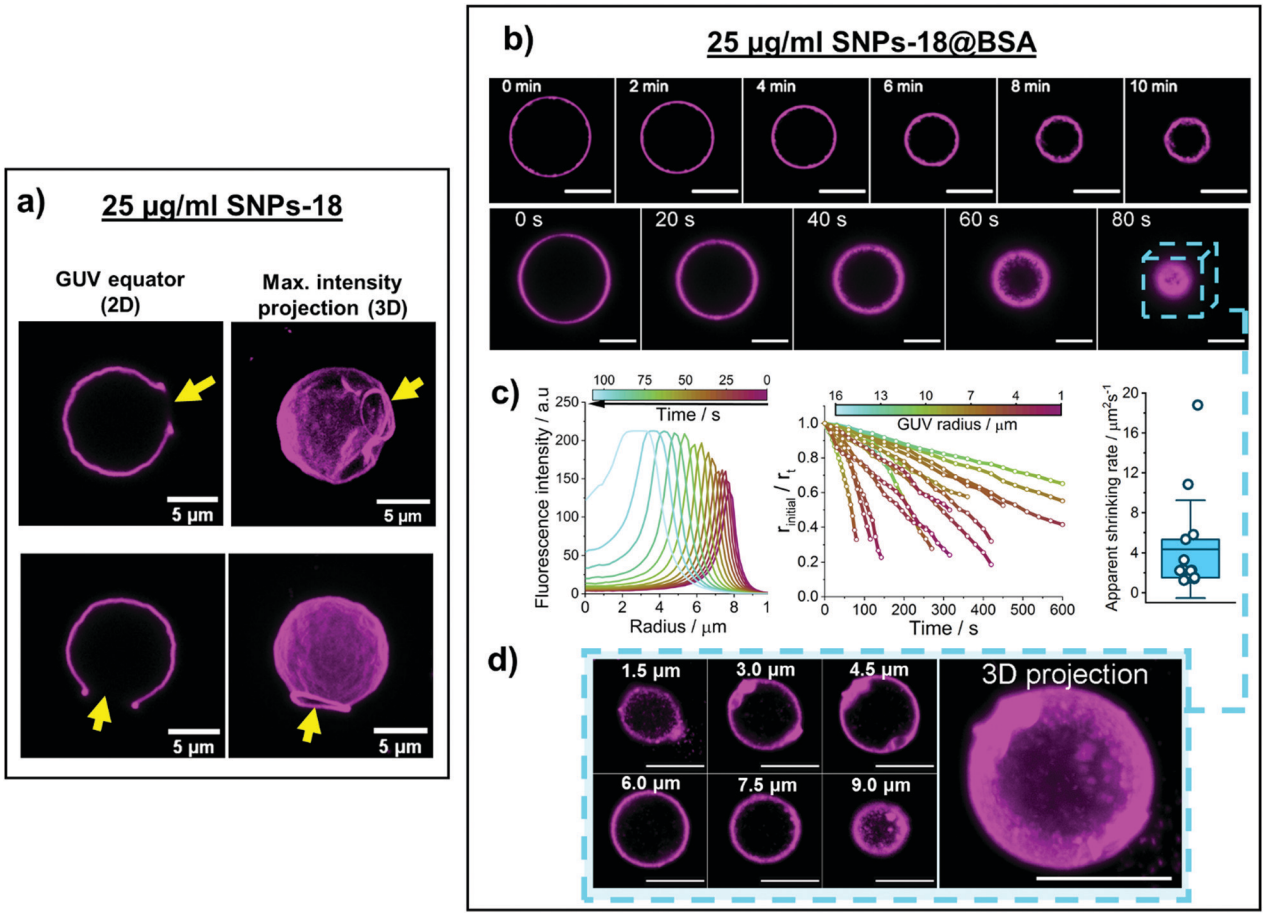

Fig. 1 Effect of the interaction of SNPs-18 and SNPs-18@BSA with DOPC GUVs. (a) Confocal microscopy images of DOPC GUVs showing permanent micro-sized pores (yellow arrows) after exposure to 25 µg ml^{-1} SNPs-18. Left micrographs show the GUVs at the equator plane and images on the right show 3D maximum intensity projections. (b) Confocal microscopy time series of DOPC GUVs labelled with Rh-DOPE show a gradual shrinkage of the vesicles accompanied by an increase in membrane thickness and fluorescence intensity. (c) Left plot is an example of radial integrated fluorescence intensity measurement of a GUV interacting with SNPs-18@BSA. The radius of the GUV decreases with time (see colour bar) and the fluorescence intensity increases. The wider curves at longer times indicate an apparent increase in membrane thickness. The middle plot shows the apparent shrinking rate of individual GUVs. The *y*-axis represents the normalised GUV radius at each time point and the colour of the lines indicate the actual radius of the GUV (see colour bar). The plot on the right shows the apparent shrinking rate distribution (the box indicates the range between the 25th and 75th percentile, the line in the box is the mean, the whiskers are the SD of the mean and the circles indicate individual data points). (d) Confocal microscopy images of a GUV after SNPs-18@BSA-induced shrinkage at different focal planes (*z*-planes) and maximum intensity projection. The GUV appears damaged but still maintains its spherical shape. Scale bar in (b) and (d) are 10 µm.

 This journal is © The Royal Society of Chemistry 2022

Open Access Article. Published on 14 June 2022. Downloaded on 11/5/2025 4:19:57 PM.
This article is licensed under a Creative Commons Attribution 3.0 Unported Licence.

the adhesion of BSA to the SNP surface creating a protein corona. The small peaks displayed in the SNPs@BSA samples correspond to free BSA molecules in solution. As observed for the bare SNPs, the hydrodynamic size of SNPs-18@BSA and SNPs-30@BSA also remains stable for at least 48 hours (Fig. S2, ESI†). This stable protein corona likely indicates a high affinity of BSA for the SNPs, where they get strongly bound, covering their surface completely. BSA has a prolate shape ($4 \times 4 \times 14$ nm)[16] and so these increased hydrodynamic diameters are consistent with either a single layer of BSA with its long-axis perpendicular to the NP surface, or a layered coverage 2–3 proteins thick. This complete surface coverage of SNPs by strongly bound proteins has been reported previously.[14,17] The ζ-potential barely changes after incubating the SNPs with BSA for 24 h (SNPs-30@BSA = -20.4 ± 0.2 mV and SNPs-18@BSA = -17.1 ± 1.8 mV) (Fig. S2c, ESI†).

Then we studied the effect of a protein corona on the interplay between SNPs of two different sizes and DOPC giant unilamellar vesicles (GUVs). For this purpose, we employed confocal laser-scanning microscopy to visualise morphological changes experienced by DOPC GUVs labelled with either 0.5 mol% Rh-DOPE or 1 mol% DiO after exposure to SNPs-18, SNPs-18@BSA, SNPs-30 and SNPs-30@BSA. GUVs were prepared by the electroformation method.[18] All experiments were carried out at a SNPs concentration of 25 μg ml^{-1}. Control experiments confirmed that the morphology of the GUVs is not affected by the presence of BSA in the medium at the concentration (0.25 mg ml^{-1}) at which they are found in the SNPs-18@BSA and SNPs-30@BSA samples (Fig. S3, ESI†).

Upon interaction with SNPs-18, the GUVs become wrinkled and show permanent microsized pores (Fig. 1(a)). At the edge of the microsized pores, we observe enhanced fluorescence intensity due to the high curvature adopted by the membrane, which appears to be rolled up (Fig. 1(a)). The formation of these large pores by this type of SNPs has previously been reported by Zhang *et al.*, who showed that this effect was accompanied by a considerable decrease in lipid lateral diffusion.[19] They proposed that the interaction of the SNPs-18 with the membrane produces a change in the tilt angle of the P^{-}–N^{+} dipole in the PC headgroup of the lipids, which would produce a denser lipid packing and consequently decrease the membrane fluidity and increase the membrane tension. This increased lateral tension generates elastic stress which is released by the fracture of the membrane, which leads to the formation of single micro-sized holes in the GUVs.[19]

Unlike SNPs-18, SNPs-18@BSA induce a gradual shrinkage of the GUVs, which eventually result in considerably smaller vesicles with a thick, crumpled membrane. Real-time confocal microscopy images show that the size of the GUVs decreases over time while their membrane becomes thicker and its fluorescence more intense (Fig. 1(b) and (c)). The increase in membrane thickness and fluorescence intensity likely denotes that SNPs-18@BSA are wrapped and generate highly curved sub-micrometre membrane invaginations. However, these curved membrane buds do not detach from the parent GUV as spots of fluorescence signifying lipid wrapped NPs were not observed in the vesicle lumen. Moreover, nano-sized pores are expected to form on the membrane allowing the contents in the lumen to be expelled from the GUVs while they shrink.

The analysis of the vesicle size against time shows a progressive shrinkage, which suggests that the adhesion of SNPs-18@BSA to the GUVs induces a slow, gradual rearrangement of the membrane. At the end of the process, the apparent radius of the vesicles is between 30% and 70% smaller compared to the radius of the initial GUV. Note that the decrease in apparent radius is a combination of a genuine decrease in vesicle radius and a drift in the focal plane through the spherical GUV as it shrinks. Three-dimensional *z*-projections indicate that the GUVs exposed to SNPs-18@BSA retain an approximately spherical shape and do not fully collapse (Fig. 1(d)). From the analysis of 14 GUVs, the average shrinking rate of the vesicle surface area was 4.4 ± 4.9 μm^2 s^{-1}. Most of the GUVs observed show an apparent shrinking rate that varies between 1.2 μm^2 s^{-1} and 5.8 μm^2 s^{-1}, but two isolated events show significantly faster (10.8 μm^2 s^{-1} and 18.8 μm^2 s^{-1}) shrinking rate (Fig. 1(c)). The variability in shrinking rate likely arises from a combination of variable membrane tension that resists the membrane wrapping the NPs and the rate of stochastic nanoscale pore formation to allow rapid water transport for the GUV to reduce its volume.

Zuraw-Weston *et al.* modulated the adhesion strength of NPs to the membrane by changing the surface charge of the latter.[20] In the strong adhesion regime, they observed a multi-stage vesicle destruction process. Firstly, the membrane wraps the NPs, inducing a gradual shrinkage of the GUVs as well as the formation of highly curved structures at their surface. Fast-shrinking vesicles can surpass a tension threshold that triggers the opening of a large permanent pore, similar to the ones induced by SNPs-18.[20] Comparing their observations with ours, this can be rationalised by the contact of SNPs-18 with the GUVs driving them to rapidly shrink and consequently transition into the permanent pore configuration, apparently skipping the first stage. For the SNPs-18@BSA, the BSA corona may be expected to decrease the interaction strength and would also increase the NP size, hence slowing down the shrinkage rate and preventing the membrane tension from reaching the lysis threshold.

Nevertheless, we do not see any evidence of a multistage interaction process for SNPs-18: membrane wrapping does not appear to be significant for these SNPs. Here, as also observed by Zhang *et al.*,[19] we only observe the rapid pore opening event and simultaneous wrinkling of the membrane as the membrane transitions from fluid to solid mechanics in a process akin to a first order phase transition. The BSA corona increases the size of these SNPs above the critical diameter for spontaneous wrapping, that for SNPs interacting with DOPC membranes has been estimated to be 25–40 nm,[19,21] making membrane bending more energetically favourable. Thus, the BSA corona on these SNPs modifies the interaction mechanism so the membrane now wraps the NPs and creates highly curved membrane structures, where gentle shrinkage of the GUVs is facilitated by nanoscale membrane pores.

The exposure of DOPC GUVs to SNPs-30 leads to completely different outcomes. Real-time confocal microscopy images

Open Access Article. Published on 14 June 2022. Downloaded on 11/5/2025 4:19:57 PM.
This article is licensed under a Creative Commons Attribution 3.0 Unported Licence.

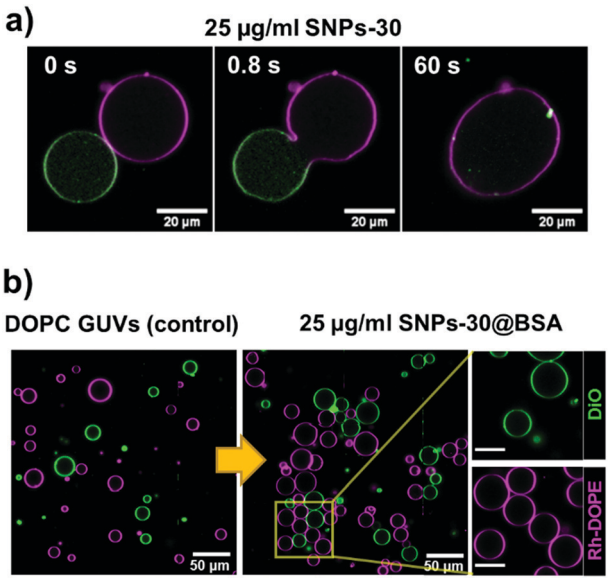

Fig. 2 Effect of the interaction of SNPs-30 and SNPs-30@BSA with DOPC GUVs. GUVs are labelled with Rh-DOPE (magenta) or DiO (green). (a) Time series of GUVs undergoing full membrane fusion after interacting with 25 μg ml^{-1} SNPs-30. (b) DOPC GUVs before and after incubation with SNPs-30@BSA for 30 min. After incubation with SNPs-30@BSA, the GUVs weakly adhere into clusters but maintain their integrity and do not fuse. On the right, zoomed in image of the region delimited by the yellow box showing each imaging channel (Rh-DOPE and DiO) separately. There is no colocalisation of dyes in the same membrane, indicating the absence of lipid mixing between GUVs labelled with different probes.

show that the interaction between SNPs-30 with two apposed GUVs induces the fusion of the vesicles. This generates a final GUV with a membrane composed of a mixture of the lipids from the two initial vesicles (Fig. 2(a)). Recently, we reported the fusogenic properties of these SNPs and proposed a mechanistic explanation for the fusion process.[21] The size of these NPs is within a critical range where the adhesion energy between the NP and membrane approximately balances the bending energy of the membrane to wrap the NP. Therefore, these SNPs induce a combination of membrane curvature and increased membrane tension that can facilitate fusion between neighbouring membranes. Membrane tension then dictates the intermediate states formed during the vesicle fusion process.[21]

The fusogenic ability of SNPs-30 is suppressed by the BSA corona. The interaction between SNPs-30@BSA promotes the adhesion of GUVs, which form clusters of tens of vesicles (Fig. 2(b)). The GUVs maintain their integrity and neither membrane perturbations nor fusion events are observed. To investigate whether fusion or hemifusion can occur between GUVs, we mixed two GUV populations labelled with Rh-DOPE or DiO respectively. These GUVs were incubated with 25 μg ml^{-1} SNPs-30@BSA for 30 min. After this time, vesicles were observed to adhere but we could not detect any transfer of fluorescent lipids between the oppositely labelled GUVs (Fig. 2(b)). These observations indicate GUV adhesion where the membrane rearrangements required for hemifusion or full fusion are suppressed. In this case, the increase in particle size due to the BSA corona likely holds the membranes apart at too great a distance for the membranes to directly interact, where sufficient membrane bending is not permitted to drive the formation of a fusion stalk with an estimated energy barrier of 20–35 k_BT.[22,23]

The BSA corona on SNPs-30 likely also reduces their adhesion energy with the membrane as membrane wrapping and vesicle collapse is no longer observed. This is despite the larger size and hence lower curvature of these NPs, which would reduce the energetic cost of membrane wrapping. This is in contrast to the SNPs-18@BSA particles, where the adhesion energy was still sufficient to promote membrane wrapping and shrinkage of GUVs. Therefore, we conclude that the curvature of the SNPs influences the assembly and structure of the BSA corona, giving different effects on the modulation of the NP adhesion energy.

Finally, we investigated the effect of SNPs with and without the BSA corona on the packing of the lipids within the

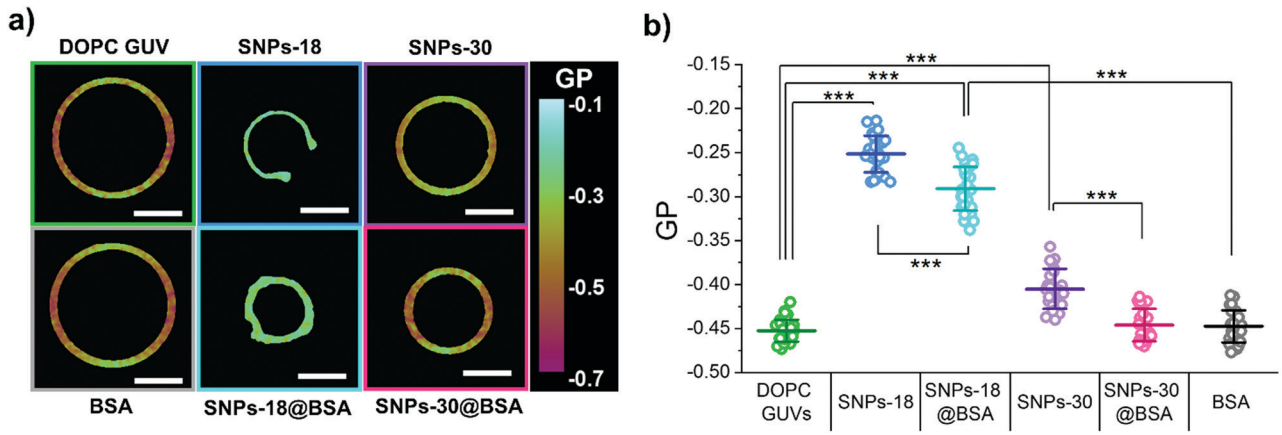

Fig. 3 Spectral imaging of DOPC GUVs labelled with Laurdan before and after exposure to 25 μg ml^{-1} SNPs with and without BSA corona. (a) Examples of Laurdan GP maps of GUVs under the different experimental conditions. Scale bars correspond to 10 μm. (b) Distribution of average Laurdan GP values for the GUVs before and after 30 min incubation with the different SNPs with and without BSA corona as well as after incubation with 0.25 mg ml^{-1} BSA. Data are presented as mean ± SD, circles indicate each individual measurement (DOPC GUVs: n = 35; SNPs-18: n = 26; SNPs-18@BSA: n = 29; SNPs-30: n = 25; SNPs-18@BSA: n = 26; BSA: n = 26). Statistical significance was tested using a one-way ANOVA with a *post-hoc* Bonferroni test (*$p < 0.1$).

 This journal is © The Royal Society of Chemistry 2022

Open Access Article. Published on 14 June 2022. Downloaded on 11/5/2025 4:19:57 PM.
This article is licensed under a Creative Commons Attribution 3.0 Unported Licence.

membrane of the GUVs using Laurdan spectral imaging. Before addition of SNPs to the sample, DOPC GUVs show an average GP value of -0.45 ± 0.01.We also performed control experiments where the DOPC GUVs were exposed to 0.25 mg ml^{-1} BSA and confirmed that the mean GP value of the GUVs remains almost identical (GP = -0.45 ± 0.02) (Fig. 3).

The exposure of the DOPC GUVs to 25 μg ml^{-1} SNPs-18 induces an increase in the mean GP to -0.25 ± 0.02 (Fig. 3), indicating that SNPs-18 produce a tighter packing of the lipids within the membrane. The lipid lateral diffusion of DOPC GUVs after interacting with these SNPs reported by Zhang *et al.* suggested a solidification of the membrane[19] but the average GP we observed is still within the GP range corresponding to liquid disordered membrane.[24,25] In our experiments, Laurdan is equally distributed along the inner and outer leaflet of the membrane so the GP values we observe correspond to the mean values of both monolayers. However, SNPs-18 suspended in the outer solution are expected to adhere primarily to the outer leaflet so their effect on the packing density of the lipids might be stronger in the outer leaflet than in the inner monolayer. In that case, the GP of the less packed inner monolayer might mask to some extent the GP value corresponding to the highly packed outer leaflet. In addition, the different lipid packing of each leaflet can lead to an intrinsic stress which gives rise to a residual bilayer tension.[26] Such differential leaflet stress could facilitate the opening of the large pores observed in the GUVs. Moreover, the asymmetric lipid packing might contribute to generate a spontaneous curvature at the pore edge which bends the membrane towards the outside of the GUV creating a rolled structure at the rim of the pore which could contribute to the stabilisation of such pores.[27] The average Laurdan GP of the GUVs after exposure to SNPs-18@BSA also indicates an increase of lipid packing in the membrane (GP = -0.29 ± 0.02) but, compared to the pristine SNPs-18, this effect is slightly weakened by the BSA corona (Fig. 3).

The effect of the larger SNPs-30 induce only a mild but statistically significant increase in the average GP of the Laurdan molecules embedded in the membrane (GP = -0.40 ± 0.02) (Fig. 3). These changes in the membrane order can lead to localised lipid packing defects, which have been previously considered as an initial step that facilitates the beginning of the fusion of adjacent lipid membranes.[21,28–30] On the contrary, the mean Laurdan GP of the GUVs remains unchanged after exposure to SNPs-30@BSA (GP = -0.45 ± 0.02) (Fig. 3). Hence, the potential contact of SNPs-30@BSA with the membrane would not induce any packing defect and consequently the GUVs remain closely apposed but their membranes do not merge.

Overall, these data suggest the BSA corona weakens the interaction between the SNPs and the membrane. In agreement with our observations, the weakening effect of protein coronas on the interaction of SNPs with supported lipid bilayers, lipid vesicles and cellular uptake has been reported before.[31–34] NPs of different chemical compositions, such as gold and polystyrene, have also exhibited reduced membrane activity and cellular uptake when coated with protein coronas[35,36] and molecular simulations have also suggested a weakening effects of the protein corona on the interaction between polystyrene nanoparticles and zwitterionic lipid membranes.[37] However, the magnitude of the effect of the BSA corona may subtly depend on the surface properties of the NP onto which they absorb, which influences the structure and assembly of this protein coat.

In conclusion, our results show the profound impact of a BSA corona on the response of DOPC GUVs to the exposure to SNPs. This effect is however different depending on the size of the pristine SNPs. It is generally accepted that the mechanism of interaction between NPs and lipid membranes is primarily determined by three main features: the size of the NPs, the adhesion strength of the NPs to the membrane and the resistance of the membrane to be deformed.[38] This implies that changes in any of these properties can result in different interaction mechanisms and therefore diverse membrane responses. Here, we have seen that the BSA corona around the SNPs significantly increases the hydrodynamic size of the bare SNPs. In addition, Laurdan spectral imaging shows a reduced ability of the SNPs@BSA to alter the lipid packing compared to the bare SNPs, which might indicate a weakening of adhesion strength of the SNPs to the membrane induced by the BSA corona. Together, the larger size and the weaker adhesion force induced by the protein corona might be responsible for the transition from the generation of large permanent membrane pores to a membrane wrapping regime in the case of the smaller SNPs-18 and for the suppression of the fusogenic activity of SNPs-30.

Additionally, the binding affinity of proteins to nanomaterials depends principally on the type of protein, the surface properties of the NPs and their size.[2,3,39] The different membrane responses produced by the two types of SNPs@BSA might therefore be related to differences in the protein corona formed on the surface of NPs of different sizes but it also suggests that even after the corona is formed, the inherent NP properties still influence the membrane interaction. This may be rationalised by the fact that the corona is physisorbed on the NP surface and therefore the BSA might be partially displaced by the SNP–lipid interaction on the membrane surface.

While simplified systems provide fundamental knowledge on biophysical and biochemical processes, further studies with more complex coronas made of different proteins and other relevant biomacromolecules are needed to understand and predict the fate of NPs within biological systems. This knowledge is critical to the eventual goal of being able to fabricate safe-by-design nanomaterials that retain their desired functions in complex biological media without causing harmful side effects.

Data availability

The data sets that support the findings of this study are available in the White Rose repository with the identifier https://doi.org/10.5518/1171.

Conflicts of interest

The authors declare no conflicts of interest.

Open Access Article. Published on 14 June 2022. Downloaded on 11/5/2025 4:19:57 PM.
This article is licensed under a Creative Commons Attribution 3.0 Unported Licence.

Acknowledgements

The authors thank Dr Nicole Hondow (School of Chemical and Process Engineering, University of Leeds) for the acquisition of the TEM images of the nanoparticles. M. A. P. is grateful to the University of Leeds for funding through the Lowson Scholarship.

References

1 J. G. Croissant, K. S. Butler, J. I. Zink and C. J. Brinker, *Nat. Rev. Mater.*, 2020, **5**, 886–909.
2 M. P. Monopoli, C. Aberg, A. Salvati and K. A. Dawson, *Nat. Nanotechnol.*, 2012, **7**, 779–786.
3 T. Cedervall, I. Lynch, S. Lindman, T. Berggard, E. Thulin, H. Nilsson, K. A. Dawson and S. Linse, *Proc. Natl. Acad. Sci. U. S. A.*, 2007, **104**, 2050–2055.
4 V. H. Nguyen and B. J. Lee, *Int. J. Nanomed.*, 2017, **12**, 3137–3151.
5 F. J. Wang, L. Yu, M. P. Monopoli, P. Sandin, E. Mahon, A. Salvati and K. A. Dawson, *Nanomedicine*, 2013, **9**, 1159–1168.
6 H. Yin, R. Chen, P. S. Casey, P. C. Ke, T. P. Davis and C. Y. Chen, *RSC Adv.*, 2015, **5**, 73963–73973.
7 J. S. Gebauer, M. Malissek, S. Simon, S. K. Knauer, M. Maskos, R. H. Stauber, W. Peukert and L. Treuel, *Langmuir*, 2012, **28**, 9673–9679.
8 D. Mahl, C. Greulich, W. Meyer-Zaika, M. Koller and M. Epple, *J. Mater. Chem.*, 2010, **20**, 6176–6181.
9 C. R. Anderson, Y. D. M. Gnopo, F. Gambinossi, S. E. Mylon and J. K. Ferri, *J. Biomed. Mater. Res., Part A*, 2018, **106**, 1061–1071.
10 M. Barbalinardo, F. Caicci, M. Cavallini and D. Gentili, *Small*, 2018, **14**, 1801219.
11 R. Garcia-Alvarez and M. Vallet-Regi, *Nanomaterials*, 2021, 11.
12 K. Nienhaus and G. U. Nienhaus, *Curr. Opin. Biomed. Eng.*, 2019, **10**, 11–22.
13 A. E. Nel, L. Madler, D. Velegol, T. Xia, E. M. V. Hoek, P. Somasundaran, F. Klaessig, V. Castranova and M. Thompson, *Nat. Mater.*, 2009, **8**, 543–557.
14 H. Y. Zhang, J. X. Peng, X. Li, S. J. Liu, Z. Y. Hu, G. J. Xu and R. A. Wu, *Colloids Surf., B*, 2018, **167**, 220–228.
15 H. Mohammad-Beigi, Y. Hayashi, C. M. Zeuthen, H. Eskandari, C. Scavenius, K. Juul-Madsen, T. Vorup-Jensen, J. J. Enghild and D. S. Sutherland, *Nat. Commun.*, 2020, 11.
16 A. K. Wright and M. R. Thompson, *Biophys. J.*, 1975, **15**, 137–141.
17 M. P. Monopoli, D. Walczyk, A. Campbell, G. Elia, I. Lynch, F. B. Bombelli and K. A. Dawson, *J. Am. Chem. Soc.*, 2011, **133**, 2525–2534.
18 M. I. Angelova, S. Soleau, P. Meleard, J. F. Faucon and P. Bothorel, *Trends in Colloid and Interface Science VI*, 1992, **89**, 127–131.
19 S. W. Zhang, A. Nelson and P. A. Beales, *Langmuir*, 2012, **28**, 12831–12837.
20 S. Zuraw-Weston, D. A. Wood, I. K. Torres, Y. Lee, L. S. Wang, Z. W. Jiang, G. R. Lazaro, S. Y. Wang, A. A. Rodal, M. F. Hagan, V. M. Rotello and A. D. Dinsmore, *Nanoscale*, 2019, **11**, 18464–18474.
21 M. Arribas Perez and P. A. Beales, *Langmuir*, 2021, **37**, 13917–13931.
22 R. J. Ryham, T. S. Klotz, L. H. Yao and F. S. Cohen, *Biophys. J.*, 2016, **110**, 1110–1124.
23 Y. G. Smirnova, S. J. Marrink, R. Lipowsky and V. Knecht, *J. Am. Chem. Soc.*, 2010, **132**, 6710–6718.
24 M. Amaro, F. Reina, M. Hof, C. Eggeling and E. Sezgin, *J. Phys. D: Appl. Phys.*, 2017, 50.
25 E. Sezgin, D. Waithe, J. B. de la Serna and C. Eggeling, *ChemPhysChem*, 2015, **16**, 1387–1394.
26 A. Hossein and M. Deserno, *Biophys. J.*, 2020, **118**, 624–642.
27 Y. Sakuma, T. Taniguchi and M. Imai, *Biophys. J.*, 2010, **99**, 472–479.
28 S. A. Akimov, R. J. Molotkovsky, P. I. Kuzmin, T. R. Galimzyanov and O. V. Batishchev, *Int. J. Mol. Sci.*, 2020, 21.
29 G. Meher and H. Chakraborty, *J. Membr. Biol.*, 2019, **252**, 261–272.
30 M. A. Tahir, Z. P. Guven, L. R. Arriaga, B. Tinao, Y. S. S. Yang, A. Bekdemir, J. T. Martin, A. N. Bhanji, D. Irvine, F. Stellacci and A. Alexander-Katz, *Proc. Natl. Acad. Sci. U. S. A.*, 2020, **117**, 18470–18476.
31 A. Lesniak, F. Fenaroli, M. R. Monopoli, C. Aberg, K. A. Dawson and A. Salvati, *ACS Nano*, 2012, **6**, 5845–5857.
32 X. Wei, X. Qu, L. Ding, J. Hu and W. Jiang, *Environ. Pollut.*, 2016, **219**, 1–8.
33 J. W. Choi, I. Y. Kim, M. Kwak, J. Kim, S. Yoon, H. J. Jang, T. G. Lee and M. B. Heo, *Micro Nano Lett.*, 2022, **17**, 59–67.
34 D. Di Silvio, M. Maccarini, R. Parker, A. Mackie, G. Fragneto and F. B. Bombelli, *J. Colloid Interface Sci.*, 2017, **504**, 741–750.
35 C. Montis, D. Maiolo, I. Alessandri, P. Bergese and D. Berti, *Nanoscale*, 2014, **6**, 6452–6457.
36 L. Wang, N. Hartel, K. X. Ren, N. A. Graham and N. Malmstadt, *Environ. Sci.: Nano*, 2020, **7**, 963–974.
37 H. Lee, *Langmuir*, 2021, **37**, 3751–3760.
38 R. Lipowsky and H. G. Dobereiner, *Europhys. Lett.*, 1998, **43**, 219–225.
39 M. Lundqvist, J. Stigler, G. Elia, I. Lynch, T. Cedervall and K. A. Dawson, *Proc. Natl. Acad. Sci. U. S. A.*, 2008, **105**, 14265–14270.

 This journal is © The Royal Society of Chemistry 2022